Journal of Alloys and Compounds 509 (2011) 391–395

Contents lists available at ScienceDirect

Journal of Alloys and Compounds

journal homepage: www.elsevier.com/locate/jallcom

Luminescence of complex ion WO_{12}^{18-} in Dy^{3+} doped nanocrystal Gd_6WO_{12} phosphor

Tingting Yu[a,b], Jiashi Sun[a,*], Ruinian Hua[b], Lihong Cheng[a], Haiyang Zhong[a], Xiangping Li[a], Hongquan Yu[c], Baojiu Chen[a,*]

[a] Department of Physics, Dalian Maritime University, Dalian, 116026, PR China
[b] College of Life Science, Dalian Nationalities University, Dalian, 116600, PR China
[c] College of Environmental and Chemical Engineering, Dalian Jiaotong University, Dalian, 116028, PR China

ARTICLE INFO

Article history:
Received 18 May 2010
Received in revised form 4 September 2010
Accepted 8 September 2010
Available online 17 September 2010

Keywords:
Tungstate
Dy^{3+}
Complex ion
Luminescence

ABSTRACT

Nanocrystal Gd_6WO_{12} phosphor doped with Dy^{3+} was prepared by a co-precipitation method. X-ray diffraction (XRD), scanning electron microscopy (SEM) and selected area electron diffraction (SAED) were used to characterize the structure and morphology of the resultant phosphor. It was found that the phosphor exists in tetragonal phase and the phosphor particles show sphere-like shape with an average size of 31 nm. In aid of excitation and emission spectra, the energy levels of the complex ion WO_{12}^{18-} were confirmed, and that the possible luminescent mechanisms for various wavelengths excitation were analyzed. The cross relaxation and energy transfer between complex ion and Dy^{3+} were discussed. The dependence of luminescent intensity and color coordinates on the excitation wavelength was also investigated.

1. Introduction

Complex ions are important luminescent centers for the luminescent materials [1–4]. The luminescent materials containing complex ions have received much attention and wide applications [5–10]. Amongst the materials containing complex ions, the scheelite and perovskite compounds have long been known as luminophors for several decades [11,12]. The scheelite compounds have a general molecular formula A_mBO_4, where A is a monovalent, divalent or trivalent metallic ion, m is the number of the metallic ion A, and B is W^{6+}, Mo^{6+} or V^{5+}. Simplest perovskite compounds have a general molecular formula ABO_3 with a metallic ion on its site A and a transition metallic ion, such as Ti^{4+}, Zr^{4+}, Nb^{5+} and Ta^{5+}, on site B.

Tungstates can be either scheelite (typical example: $CaWO_4$) or peroveskite (typical example: Bi_2WO_6) compounds. The luminescence of the complex ions WO_4^{2-} and WO_6^{6-} was widely studied [13–18]. The luminescent mechanism of the complex ions WO_4^{2-} and WO_6^{6-} was assigned to the charge transfer from oxygen 2p orbital to the 5d orbital of W^{6+}. In this case, the energy levels include one ground state $^1A_1$ and four excited states $^1T_1$, $^1T_2$, $^3T_1$ and $^3T_2$ (the energy level scheme will be shown in Fig. 4). In general, the emission corresponding to the spin-forbidden transition $^3T_1 \rightarrow {}^1A_1$ can be observed thanks to the fact that spin-forbidden selective rule is broken by the spin-orbital interaction. However, the absorption transition from $^1A_1$ to $^3T_1$ cannot easily be observed in the excitation spectrum due to the spin-forbidden rule. The strong absorption band in the near ultraviolet region is assigned to the transition $^1A_1 \rightarrow {}^1T_1$.The transition $^1A_1 \rightarrow {}^1T_2$ is usually overlapped with the host absorption band [19]. The absorption and emission wavelengths depend on the specific type of tungstate compounds since the energy level locations are various in different hosts. Therefore, exploring novel complex ions activated phosphors, which can be excited by various excitation sources, would be an interesting issue.

In this paper, nanocrystal Gd_6WO_{12} phosphor doped with Dy^{3+} was prepared via a co-precipitation route. The crystal structure and morphology of the obtained phosphor were examined through XRD, SEM and SAED. The luminescent properties of the sample were analyzed by means of fluorescence spectroscopy. The intense broad band emissions from the complex ion WO_{12}^{18-} and weak emissions from Dy^{3+} were observed. The excitation-wavelength dependences of emission intensity and the color coordinates were studied.

2. Experimental details

2.1. Synthesis

Spectrographically pure Gd_2O_3, Dy_2O_3 (99.99%) and other analytically pure reagents (99.9%) were used in the sample preparation. $GdCl_3{\cdot}6H_2O$ and $DyCl_3{\cdot}6H_2O$ were obtained via a re-crystallization process. First, Gd_2O_3 and Dy_2O_3 were dis-

* Corresponding authors. Tel.: +86 411 84728909; fax: +86 411 84728909.
E-mail addresses: jiashi.sun@gmail.com (J. Sun), chenmbj@sohu.com (B. Chen).

0925-8388/$ – see front matter © 2010 Elsevier B.V. All rights reserved.
doi:10.1016/j.jallcom.2010.09.040

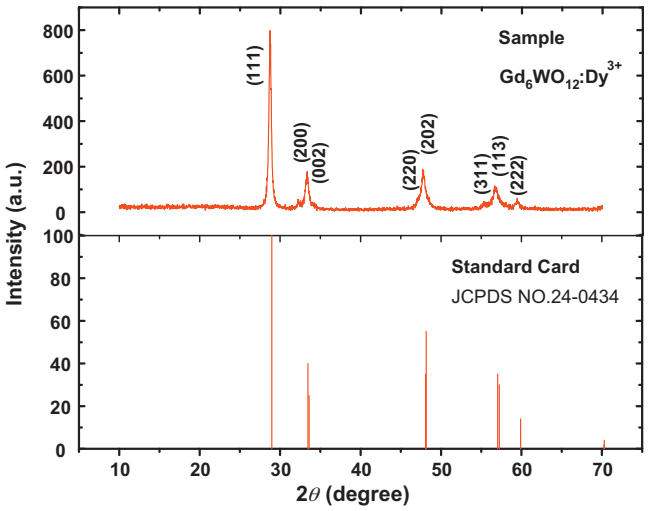

Fig. 1. XRD pattern of nanocrystal Gd_6WO_{12} phosphor doped with 1 mol% Dy^{3+}.

solved, respectively, in hydrochloric acid solutions, and then the $GdCl_3{\cdot}6H_2O$ and $DyCl_3{\cdot}6H_2O$ were received by re-crystallizing the solutions for five times.

Nanocrystal $Gd_6WO_{12}:Dy^{3+}$ phosphor was synthesized via a co-precipitation reaction. Firstly, certain amount of $GdCl_3{\cdot}6H_2O$ and $DyCl_3{\cdot}6H_2O$ was mixed based on a molar ratio of 99:1 (Gd^{3+} to Dy^{3+}) and dissolved in 10 ml deionized water. Meanwhile, appropriate amount of $Na_2WO_4{\cdot}2H_2O$ was dissolved in 30 ml deionized water, and its pH was adjusted to a certain value with ammonia under magnetic stirring at room temperature. Secondly, the solution with rare earth (RE) ions was poured into $Na_2WO_4{\cdot}2H_2O$ solution drop by drop under magnetic stir. The white precipitation was observed during the pouring and stirring process. After the solution was completely poured into $Na_2WO_4{\cdot}2H_2O$ solution, the white suspension solution was stirred unceasingly for 30 min to ensure that the reaction was completed. Thirdly, the obtained emulsion mixture was centrifuged at 6000 rpm for 20 min. The precipitation was washed by using deionized water for three times, and then dried at 100 °C for 3 h. Finally, the dried product was calcined at 900 °C for 4 h to obtain the nanosized $Gd_6WO_{12}:Dy^{3+}$ phosphor. In the synthesis process, it was found that the pH value of Na_2WO_4 solution and the mole ratio of W^{6+} to RE^{3+} greatly affect the formation of the product. The pure phase $Gd_6WO_{12}:Dy^{3+}$ can be gotten while the pH value is higher than 12 and the ratio of W^{6+} to RE^{3+} is 1.5:1. A detailed preparative procedure can be found in our previous work [20].

2.2. Characterization

The crystal structure of the sample was characterized by using a SHIMADZU XRD (X-ray diffraction)-6000 X-ray diffractometer with Cu Kα1 radiation (λ=1.5406 Å) source. The scanning region of 2θ angle is from 10° to 70° with step size of 0.02°. The morphology and particle size were characterized by using a HITACHI S-4800 field-emission scanning electron microscope (FE-SEM). The image of SAED was taken on a Transmission Electron Microscope (TEM) JEOL JEM 2100. Emission and excitation spectra were recorded by Hitachi F-4600 fluorescence spectrometer equipped with 150 W Xe lamp as an excitation source. Prior to spectral measurements, a calibration procedure was run by using the standard accessories offered by the manufacturer. The excitation spectra were intensity-calibrated in the region 200–600 nm, and the emission spectra were also intensity-calibrated in the region 200–900 nm.

3. Results and discussion

3.1. Structure and morphology characterization

The XRD pattern for the obtained nanocrystal Gd_6WO_{12} phosphor doped with 1 mol% Dy^{3+} is shown on the top of Fig. 1, and the diffraction pattern for the tetragonal phase Gd_6WO_{12} reported in JCPDS card No. 24-0434 is shown at the bottom. It can be seen that the diffraction peak positions in these two patterns are in good agreements. This fact means that the obtained resultant from our synthesis experiment is pure phase Gd_6WO_{12}. The broadening of diffraction peaks in the studied sample is caused by the small size of the phosphor particles. The crystallographic size of the nanoparticles can be estimated by using Scherrer formula expressed below,

$$D = \frac{k\lambda}{(\beta^2 - \beta_0^2)^{1/2}\cos\theta}$$

$k = 0.9$, λ (0.15406 nm) is the Kα radiation wavelength of copper target, β is the full width at half maximum (FWHM) of the diffraction peak, β_0 is a modification factor for the system broadening, and θ stands for half of the diffraction position 2θ. In the calculation the data for the diffraction peaks at $2\theta = 28.72°$ and 33.32° were used, β_0 was taken to be 0.01° as the system broadening measured by using silicon monocrystal. The confirmed average crystallographic size is approximately 30 nm.

Fig. 2(a) shows the FE-SEM image of nanocrystal $Gd_6WO_{12}:Dy^{3+}$ phosphor. This image displays that the phosphor particles have sphere-like shape and the particle sizes distribute in a narrow scale. Fig. 2(b) represents the column graph for particle size distribution with a Gaussian's fitting curve. By counting 100 particles the average particle size was estimated to be 31 nm, which coincides with

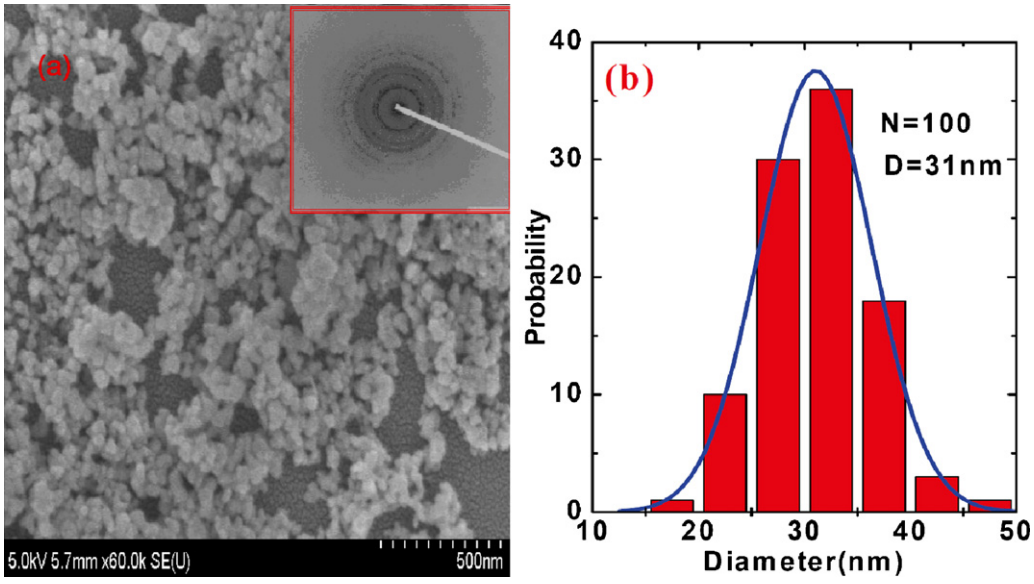

Fig. 2. (a) SEM image of nanocrystal $Gd_6WO_{12}:Dy^{3+}$ phosphor; (b) Size distribution of $Gd_6WO_{12}:Dy^{3+}$ nanoparticles. The insert in Fig. 2 (a) shows the SAED image of nanocrystal Gd_6WO_{12} phosphor.

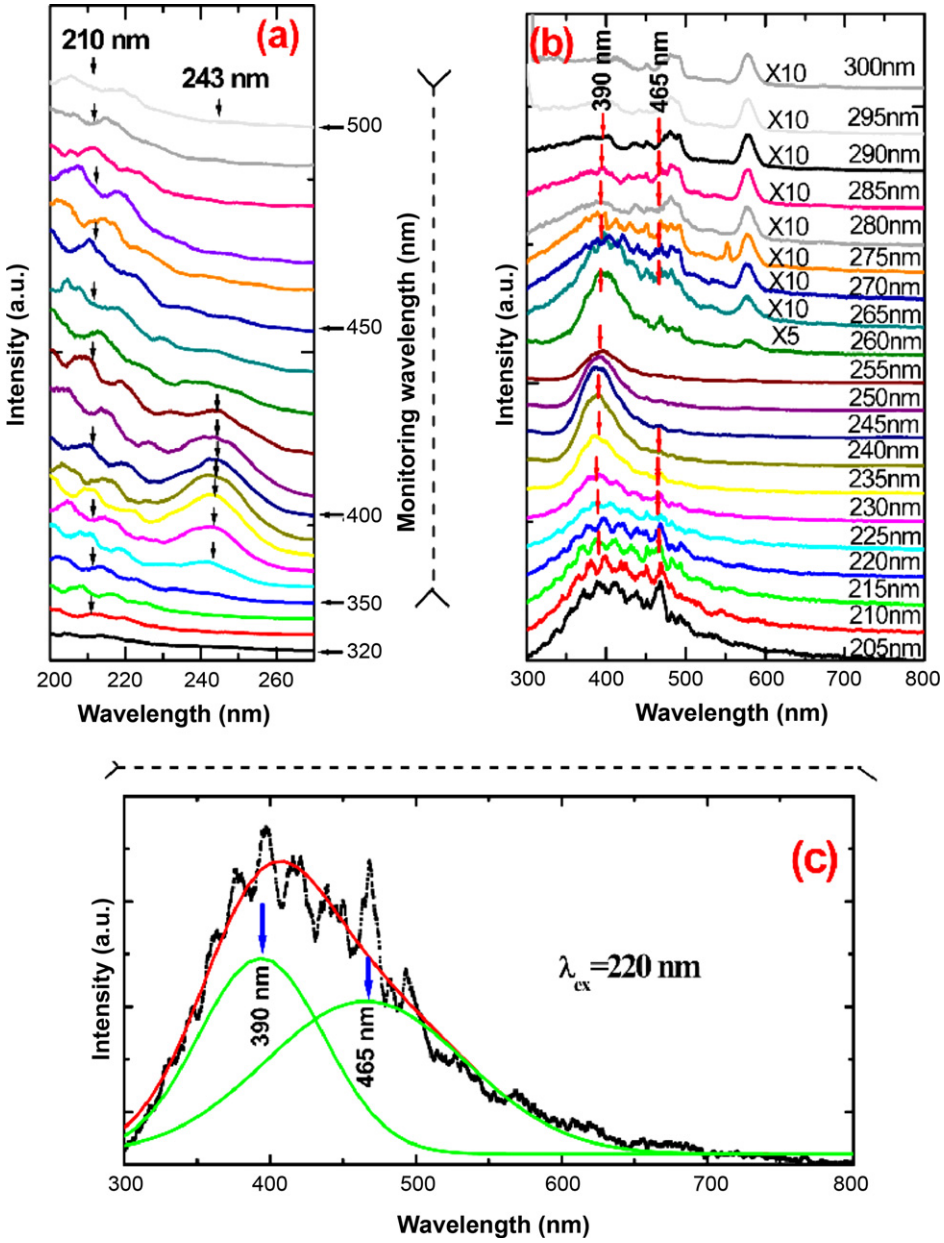

Fig. 3. (a) Excitation spectra of nanocrystal Gd_6WO_{12}:Dy^{3+} phosphor while monitoring various emission wavelengths; (b) Emission spectra of nanocrystal Gd_6WO_{12}:Dy^{3+} phosphor under various wavelengths excitation; (c) Gaussian's fitting of the emission spectra under 220 nm excitation.

the crystallographic size derived from XRD. This fact implies that the Gd_6WO_{12} particles are crystallized well [21].

In order to further check the crystal structure of the sample, the SAED image was taken and shown in Fig. 2(a) as an insert. From the diffraction pattern the distances between lattice planes can be calculated to be 0.314, 0.268, 0.189 and 0.164 nm corresponding to the diffraction circles from the inside to outside. The SAED results reveal that the prepared sample is Gd_6WO_{12}.

3.2. Luminescence of WO_{12}^{18-} and Dy^{3+} in nanocrystal Gd_6WO_{12}

The excitation spectra for the nanocrystal Gd_6WO_{12}:Dy^{3+} were measured while monitoring various emission wavelengths starting from 320 to 500 nm with an increment of 10 nm, and are shown in Fig. 3(a). It can be seen that: when the monitoring wavelength is shorter than 360 nm, only one broad excitation band centered at a wavelength shorter than 220 nm is observed; when the monitoring wavelengths fall in the region 360–430 nm, a new broad band centered at 243 nm appears and its intensity increases first and then decreases; if the monitoring wavelength is longer than 460 nm, the 243 nm band disappears. It should be noted that the intensity of 210 nm excitation band changes with monitoring wavelength and can be observed in all the excitation spectra, therefore this band can be assigned to the overlap between the absorptions of host matrix and the upper $^1T_2$ state of complex ion WO_{12}^{18-}.

Fig. 3(b) represents the emission spectra of nanocrystal Gd_6WO_{12}:Dy^{3+} phosphor for different excitation wavelengths. The excitation wavelength changes from 205 to 300 nm with a step size of 5 nm. When the excitation wavelength is shorter than 235 nm, the emission spectra exhibit a broad band which can be decomposed by Gaussian's fitting into two components centered at 390 and 465 nm as shown in Fig. 3(c), and that the intensity of 465 nm component decreases with the increase of excitation wavelength. When the excitation wavelength is located at 235–255 nm, the

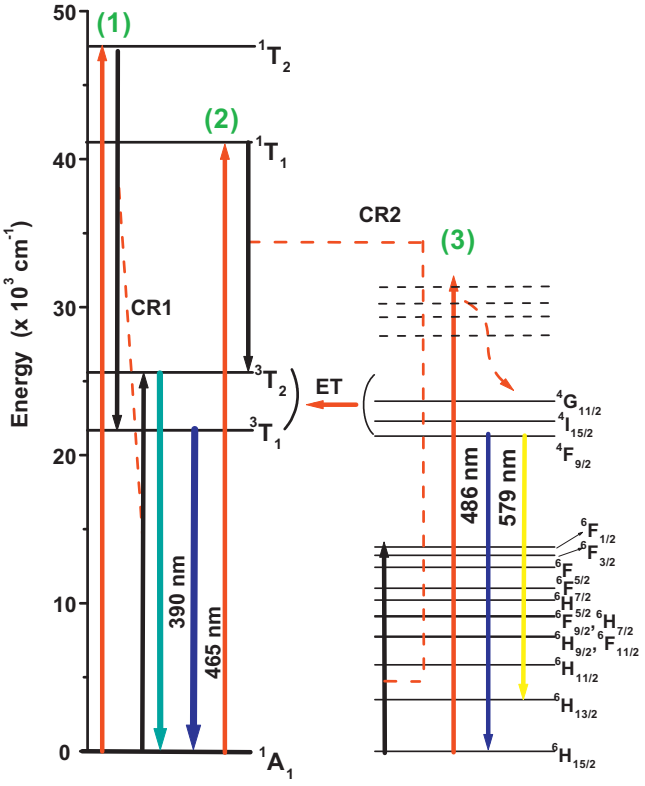

Fig. 4. The simplified energy schemes for complex ion WO_{12}^{18-} and Dy^{3+} together with the luminescent mechanisms.

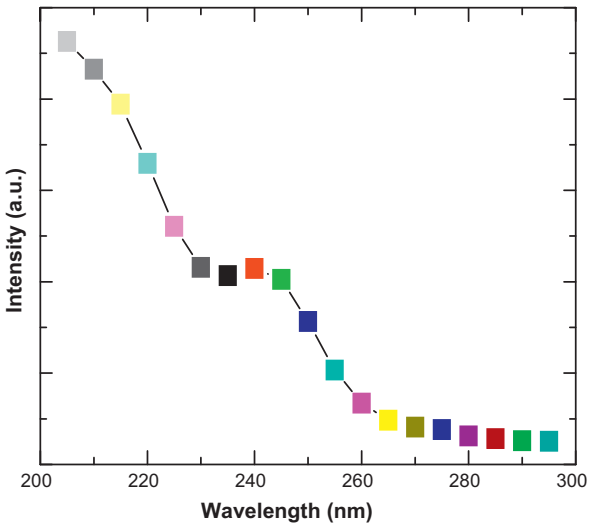

Fig. 5. Dependence of integrated emission intensity on the excitation wavelength.

465 nm component disappears, and then appears again with the increase of excitation wavelength. While the excitation wavelength is longer than 260 nm the broad band emissions and the intrinsic f–f transitions of Dy^{3+} ($^4F_{9/2} \rightarrow {}^6H_{15/2}$ peaking at 486 nm and $^4F_{9/2} \rightarrow {}^6H_{13/2}$ peaking at 579 nm) are observed, however, they are relatively weak. In order to give a clear look, the emission spectra for the excitation wavelengths ranging from 265 to 300 nm are enlarged by a factor of 10. The 465 nm emission in those emission spectra measured upon the excitation wavelengths longer than 260 nm is overlapped with Dy^{3+} emission corresponding to $^4F_{9/2} \rightarrow {}^6H_{15/2}$ transition.

From above spectral results, it can be deduced that the broad bands in the excitation and emission spectra are related with the complex ion WO_{12}^{18-} [22,23]. The 210 and 243 nm excitation peaks can be assigned to the transitions from the ground state $^1A_1$ to the upper state $^1T_2$ and $^1T_1$ of the complex ion WO_{12}^{18-}, respectively. The emission peaks located at 390 and 465 nm can be assigned to the transition from the excited state $^3T_2$ and $^3T_1$ to the ground state $^1A_1$. The simplified energy level schemes of WO_{12}^{18-} and Dy^{3+} are shown in Fig. 4. The possible luminescent mechanisms for the studied nanocrystal Gd_6WO_{12}:Dy^{3+} phosphor can be explained as follows:

When the $^1T_2$ state is excited by 210 nm light, a cross relaxation $^1T_2 + {}^1A_1 \rightarrow {}^3T_1 + {}^3T_2$ (see CR1 in Fig. 4) may happen. In this case the emissions centered at 390 and 465 nm corresponding to $^3T_2 \rightarrow {}^1A_1$ and $^3T_1 \rightarrow {}^1A_1$ can be observed as shown in Fig. 3(b).

While the excitation wavelength reaches 243 nm, the $^1T_1$ state is populated and then a cross relaxation $^1T_1 + {}^6H_{15/2}(Dy^{3+}) \rightarrow {}^3T_2 + {}^6F_{1/2}(Dy^{3+})$ (see CR2 in Fig. 4) may take place, so that 465 nm emission disappears and only 390 nm emission corresponding to $^3T_2 \rightarrow {}^1A_1$ can be detected as shown in Fig. 3(b).

However, if the excitation wavelength is longer than the absorption wavelength of $^1A_1 \rightarrow {}^1T_1$ transition and shorter than the absorption wavelength of $^1A_1 \rightarrow {}^3T_2$ transition, the complex ion WO_{12}^{18-} cannot be excited directly. In this instance, the Dy^{3+} ions at ground state can be excited with these wavelengths and reach their higher excited states, and then relax nonradiatively to $^4F_{9/2}$ via cascade multiphonon relaxations. In this case the 486 and 597 nm emissions corresponding to the transitions from $^4F_{9/2}$ to $^6H_{15/2}$ and $^6H_{13/2}$ of Dy^{3+} can be observed. Meanwhile, an energy transfer from Dy^{3+} at $^4G_{11/2}/{}^4I_{15/2}/{}^4F_{9/2}$ levels to complex ion WO_{12}^{18-} may occur, thus the 390 and 465 nm emissions corresponding to the transitions from $^3T_2$ and $^3T_1$ to $^1A_1$ can be observed. The reason why the total emission intensities are weak is due to the fact that the f–f transitions of Dy^{3+} ions are usually weak.

Since the nanocrystal Gd_6WO_{12}:Dy^{3+} phosphor shows excitation-wavelength-dependent emission spectra, the integrated emission intensity for each spectrum under corresponding wavelength excitation were calculated. Fig. 5 shows the relationship between the integrated emission intensity and the excitation wavelength. A general varied trend is clearly seen that the inte-

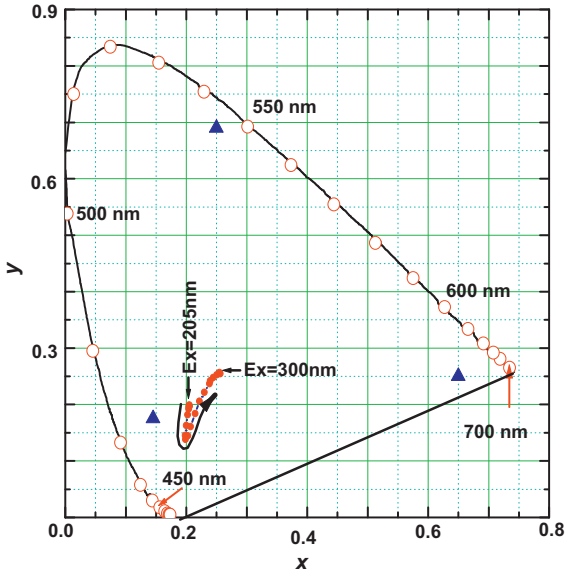

Fig. 6. Dependence of color coordinates on the excitation wavelength (the arrowed curve shows the shift trend of color coordinates with increasing excitation wavelength; 3 triangle points represent the color coordinates for standard tricolor phosphors for full color TV sets).

grated emission intensity decreases with the increase of excitation wavelength. The excitation wavelengths ranging from 200 to 260 nm are more effective for obtaining intense fluorescence. The peak located at 243 nm in this figure is due to the absorption of $^1T_1$ state of $WO_{12}{}^{18-}$ ion.

3.3. Dependence of color coordinates on excitation wavelength

Color coordinates are important factor for evaluating luminescent materials. It is already discovered that the profile and intensity of emission spectra depend on the excitation wavelength in nanocrystal Gd_6WO_{12}:Dy^{3+} phosphor. Therefore, its emissive color coordinates would be dependent on the excitation wavelength too [24]. By using the intensity-calibrated emission spectra and the color matching function issued by CIE (Commission International del'Eclairage) in 1931, the color coordinates for the sample under various wavelength excitations were calculated. The dependence of color coordinates on the excitation wavelength is shown in Fig. 6. In this figure, three triangle points indicate the color coordinates of standard tricolor phosphors for full color TV sets, the solid circles represent the color coordinates for the studied Gd_6WO_{12}:Dy^{3+} phosphor. The curve with an arrow shows the varying trend of the color coordinates with increasing excitation wavelength. It can be seen that the color coordinates first shift from blue to deep blue and then shift into the white region in the color space. This nanocrystal Gd_2WO_{12}:Dy^{3+} with the special chromatric and spectral property probably can be applied in some special fields, such as color-varied indicators, fluorescence biomarkers, and so on.

4. Conclusions

In conclusion, nanocrystal Gd_6WO_{12}:Dy^{3+} phosphor has been successfully synthesized via a co-precipitation reaction. The XRD pattern and SAED image indicated that the obtained sample is pure phase Gd_6WO_{12} and the nanocrystals exist in tetragonal phase. SEM image displayed sphere-shaped and uniformed morphology of the resultant nanoparticles. The excitation and emission spectra were measured. 210 and 243 nm absorption bands of the complex ion $WO_{12}{}^{18-}$ were observed in the excitation spectra. Intense broad band emissions centered at 390 and 465 nm originating from the complex ion $WO_{12}{}^{18-}$, weak emissions peaking at 486 and 579 nm corresponding to the transitions from $^4F_{9/2}$ to $^6H_{15/2}$ and $^6H_{13/2}$ of Dy^{3+} were observed. It was also found that the emission spectra are excitation-wavelength-dependent. The luminescent mechanism was analyzed. The excitation wavelength dependence of color coordinates was studied.

Acknowledgements

This work was partially supported by NSFC (National Natural Science Foundation of China), (Grant No. 50972021 and 50802010), Natural Science Foundation of Liaoning Province (Grant No. 20092147), Foundation of Education Department of Liaoning Province (Grant No. 2009A117), and Fundamental Research Funds for the Central Universities (Grant No. 2009QN066 and 2009JC16). One of the co-authors, HY-Zhong, wishes to gratefully acknowledge the financial support from The National High-teach Research & Development Program (863 Program) (Grant No. 2008AA06Z317).

References

[1] C.F. Guo, Y. Xu, F. Lv, X. Ding, J. Alloys Compd. 497 (2010) L21–L24.
[2] Xie An, Yuan Ximing, Wang Fengxiang, Shi Yu, Li Jian, Liu Li, Mu Zhongfei, J. Alloys Compd. 501 (2010) 124–129.
[3] X.H. He, M.Y. Guan, N. Lian, J.H. Sun, T.M. Shang, J. Alloys Compd. 492 (2010) 452–455.
[4] W.T. Sun, Y.X. Gu, Q.H. Zhang, Y.G. Li, H.Z. Wang, J. Alloys Compd. 493 (2010) 561–564.
[5] L.G. Sun, Q.R. Guo, X.L. Wu, S.J. Luo, W.L. Pan, K.L. Huang, J.F. Lu, L. R, M.H. Cao, C.W. Hu, J. Phys. Chem. C 111 (2007) 532–537.
[6] Z.L. Fu, B.K. Moon, H.K. Yang, J.H. Jeong, J. Phys. Chem. C 112 (2008) 5724–5728.
[7] Y. Tian, B.J. Chen, R.N. Hua, L.H. Cheng, H.Y. Zhong, J.S. Sun, B. Wang, J. Wan, W.L. Lu, K. Jang, J. Nanosci. Nanotechnol. 10 (2010) 1943–1946.
[8] Y. Tian, X. Qi, X. Wu, R.N. Hua, B. Chen, J. Phys. Chem. C 113 (2009) 10767–10772.
[9] N. Imanaka, S. Tamura, Y. Kobayashi, Y. Okazaki, M. Hiraiwa, T. Ueda, G. Adachi, J. Phys. Chem. C 113 (2009) 10767–10772.
[10] T. Harada, Y. Hasegawa, Y. Nakano, M. Fujiki, M. Naito, T. Wada, Y. Inoue, T. Kawai, J. Alloys Compd. 488 (2009) 599–602.
[11] T. Thongtem, S. Kungwankunakorn, B. Kuntalue, A. Phuruangrat, S. Thongtem, J. Alloys Compd. 506 (2010) 475–481.
[12] H. Hashimoto, T. Kusunose, T. Sekinob, J. Alloys Compd. 484 (2009) 246–248.
[13] L.J. Burcham, I.E. Wachs, Spectrochim. Acta Part A 54 (1998) 1355–1368.
[14] G. Blasse, G.J. Dirksen, L.H. Brixner, J. Solid State Chem. 46 (1983) 294–305.
[15] X.Y. Zhang, Z.S. Li, H. Zhang, S.X. Ouyang, Z.G. Zoum, J. Alloys Compd. 469 (2009) L6–L9.
[16] S. Rajagopal, V.L. Bekenev, D. Nataraj, D. Mangalaraj, O. Yu, Khyzhun, J. Alloys Compd. 496 (2010) 61–68.
[17] J. Chen, X.H. Gong, Y.F. Lin, Y.J. Chen, Z.D. Luo, Y.D. Huang, J. Alloys Compd. 492 (2010) 667–670.
[18] S. Rajagopal, D. Nataraj, O. Yu, Khyzhun, Y. Djaoued, J. Robichaud, D Mangalaraj, J. Alloys Compd. 493 (2010) 340–345.
[19] S. Shionoya, W.M. Yen, Phosphor handbook, CRC Press, Boca Raton, London, New York, Washington, DC, 1999, pp. 201–212.
[20] Y. Tian, B.J. Chen, R.N. Hua, H.Y. Zhong, L.H. Cheng, J.S. Sun, W.L. Lu, J. Wan, Physica B: Condens. Matter 404 (2009) 3598–3601.
[21] B.J. Chen, Q.Y. Meng, H.Y. Zhong, J.S. Sun, L.H. Cheng, Y. Peng, T. Yu, M. Chen, J. Nanosci. Nanotechnol. 8 (2008) 1165–1169.
[22] M Morita, in: S. Shionoya, Y. Toyozawa, T. Koda, H. Kukimoto (Eds.), $MoO_4{}^{2-}$, $WO_4{}^{2-}$ compounds, and one-dimensional compounds, in Hikaribussei Handbook (Handbook of Optical Properties of Solids), Asakura Shoten, Tokyo, 1984, chapter 2.12.6 and 2.19.2 (in Japanese).
[23] G. Blasse, Struct. Bond. 42 (1980) 1.
[24] B. Chen, K. Jang, H. Lee, M. Jayasimhadri, E. Cho, J. Phys. D: Appl. Phys. 42 (2009) 105401.